Molecular dynamics simulations of diffusion and clustering along critical isotherms of medium-chain *n*-alkanes

J. W. Mutoru,[1] W. Smith,[2] C. S. O'Hern,[3] and A. Firoozabadi[1,a)]
[1]*Department of Chemical and Environmental Engineering, Yale University, New Haven, Connecticut 06520-8286, USA*
[2]*Department of Physics, Yale University, New Haven, Connecticut 06520-8286, USA*
[3]*Department of Mechanical Engineering and Materials Science and Department of Physics, Yale University, New Haven, Connecticut 06520-8286, USA*

(Received 27 July 2012; accepted 5 December 2012; published online 14 January 2013)

Understanding the transport properties of molecular fluids in the critical region is important for a number of industrial and natural systems. In the literature, there are conflicting reports on the behavior of the self diffusion coefficient D_s in the critical region of single-component molecular systems. For example, D_s could decrease to zero, reach a maximum, or remain unchanged and finite at the critical point. Moreover, there is no molecular-scale understanding of the behavior of diffusion coefficients in molecular fluids in the critical regime. We perform extensive molecular dynamics simulations in the critical region of single-component fluids composed of medium-chain *n*-alkanes—*n*-pentane, *n*-decane, and *n*-dodecane—that interact via anisotropic united-atom potentials. For each system, we calculate D_s, and average molecular cluster sizes κ_{cl} and numbers N_{cl} at various cluster lifetimes τ, as a function of density ρ in the range $0.2\rho_c \leq \rho \leq 2.0\rho_c$ at the critical temperature T_c. We find that D_s decreases with increasing ρ but remains finite at the critical point. Moreover, for any given $\tau < 1.2 \times 10^{-12}$ s, κ_{cl} increases with increasing ρ but is also finite at the critical point.
 [http://dx.doi.org/10.1063/1.4773282]

I. INTRODUCTION

Molecular diffusion in the critical region has implications in supercritical extraction and other industrial and natural processes, e.g., in CO_2-flooding for enhanced oil recovery developed miscibility occurs in the critical region of the oil–CO_2 fluid. This mass transfer physico-chemical process takes place at a specific minimum miscibility pressure through multiple contacts between CO_2 and oil until a single phase is formed.[1] In this work, we systematically investigate diffusion behavior in the critical region of single-component medium-chain *n*-alkane systems, in order to set the stage for understanding of diffusion in the critical region of binary and multicomponent systems.

In single-component systems, there is no consensus on the density and temperature dependence of the self diffusion coefficient D_s in the critical region. Experimental and simulation data for D_s of hydrocarbons in the critical region are scarce. To the best of our knowledge, the only experimental data in the critical region of alkanes are for methane[2] and ethane.[3] In general, for single-component molecular fluids, there are conflicting experimental and simulation results on the behavior of D_s near the critical point.

Experimentally, Cini-Castagnoli *et al.*[4] data from capillary tube measurements show that D_s of methane decreases by $(80 \pm 20)\%$ at the critical point. Duffield and Harris[5] data from a horizontal diffusion cell, where the critical temperature was approached isochorically, show a peak in D_s in the critical region of CO_2. In contrast, data by Etesse *et al.*[6] from pulsed gradient spin-echo nuclear magnetic resonance, where the critical point was approached isothermally, show no anomalous behavior in the D_s of CO_2 in the critical region.

Drozdov and Tucker[7,8] report weak anomalous behavior of D_s from molecular dynamics (MD) simulations near the critical densities of a Lennard-Jones fluid, though their predictions have been challenged.[9] However, Das *et al.*[10] and De *et al.*[11] report that D_s does not display a detectable critical anomaly based on molecular simulations.

The inconsistencies in the literature highlight the need for a detailed examination of behavior of D_s in molecular fluids. Thus, we seek to understand diffusion in the critical region of single-component gas-liquid systems on the molecular scale. We use MD simulations to probe the microscopic dynamics of medium-chain *n*-alkanes—*n*-pentane (nC_5), *n*-decane (nC_{10}), and *n*-dodecane (nC_{12}), but we believe we would find similar results for other single-component gas-liquid systems in the critical region.

We investigate the extent to which the size and nature (whether transient or persistent) of molecular clusters control the self diffusion process in the critical region. This idea is in line with that of cluster diffusion that has been applied only in binary systems.[12] Thus, if D_s decreases towards zero at the critical point, then the average size of molecular clusters κ_{cl} diverges at the critical point, as illustrated in Figure 1 along a critical isotherm of a hypothetical single-component gas-liquid system. Otherwise, if D_s remains finite at the critical point, then κ_{cl} should be finite too.

a)Author to whom correspondence should be addressed. Electronic mail: abbas.firoozabadi@yale.edu.

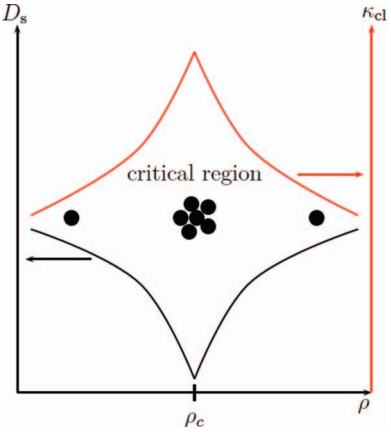

FIG. 1. A schematic of one possible scenario for the connection between the decreasing self diffusion coefficient D_s towards zero (left axis), and the diverging size of molecular clusters κ_{cl} (right axis) as the critical density ρ_c is approached along a critical isotherm of a hypothetical single-component gas-liquid system.

We study the behavior of self diffusion coefficients D_s and molecular clustering—in terms of average cluster sizes κ_{cl} and numbers N_{cl} at various cluster lifetimes τ—along critical isotherms ($T = T_c$) by varying density about the critical density ρ_c in the range $0.2\rho_c \leq \rho \leq 2.0\rho_c$. We use the critical points for nC$_5$, nC$_{10}$, and nC$_{12}$ reported by Ungerer *et al.*[13] from two anisotropic united atom (AUA) models—AUA1 and AUA2. Table I compares the reported T_c and ρ_c to the average experimental measurements for each n-alkane compiled in the National Institute of Standards and Technology (NIST) database.[14] Overall, there is good agreement between the model and experimental values. Alkanes heavier than nC$_{12}$ are not investigated in this work since their rate of thermal decomposition is significant.[15]

The rest of this paper is organized as follows: in Sec. II, we provide details of the MD simulations; in particular, the numerical algorithm (Sec. II A), the anisotropic united atom models used (Sec. II B), and the tracking of system dynamics: molecular motion, diffusion, and clustering (Sec. II C). In Sec. III A, we compare our simulation results for D_s to data from experiments. In Sec. III B, we provide results for molecular clustering in the critical region. We conclude and suggest future studies in Sec. IV.

TABLE I. Critical points of nC$_5$, nC$_{10}$, and nC$_{12}$ computed from AUA1 and AUA2 models.

n-alkane	Expt.[14]	AUA1[13]	%dev[a]	AUA2[13]	%dev
		T_c (K)			
nC$_5$	469.7	464.7	1.1	468.9	0.2
nC$_{10}$	617.7	588.3	4.7	615.7	0.3
nC$_{12}$	658.1	626.4	4.8	651.6	0.9
		ρ_c (kg/m^3)			
nC$_5$	232	247	6.5	218	6
nC$_{10}$	230	223	3	225	2.2
nC$_{12}$	227	252	11	217	4.4

[a]%dev$= \frac{|T_{c,\mathrm{sim}} - T_{c,\mathrm{exp}}|}{T_{c,\mathrm{exp}}}$%.

II. SIMULATION DETAILS

A. Numerical algorithm

We use a microcanonical ensemble to compute how motions—that describe positions and velocities—of individual atoms in a system change with time. Our MD simulations at constant number of molecules N, volume V, and energy E allow the tracking of the time evolution of a given system, e.g., as depicted in Figure 2 for a system of $N = 32$ nC$_5$ molecules, showing the changing positions of the molecules over the course of the simulation in terms of the relaxation time of the molecular length scale $t_{\sigma_{\mathrm{mol}}}$.

We study the interaction potential $u(r_1, \ldots, r_{N_a})$ from the positions of atoms $\boldsymbol{r}_i = (x_i, y_i, z_i)$ whose motion is described by integration of Newton's equations:

$$m_i \left(\frac{d^2 \boldsymbol{r}_i}{dt^2} \right) = \boldsymbol{f}_i, \tag{1}$$

where m_i, $d^2\boldsymbol{r}_i/dt^2$, and $\boldsymbol{f}_i$ are the mass, acceleration, and force acting on particle i, respectively.

The force $\boldsymbol{f}_i$ is obtained from the derivative of the potential function u with respect to each atom's degrees of freedom:

$$\boldsymbol{f}_i = -\frac{\partial u(\boldsymbol{r}^{N_a})}{\partial \boldsymbol{r}_i}. \tag{2}$$

For linear hydrocarbons, u is a summation over all occurrences of intra- and inter-molecular contributions due to bond-

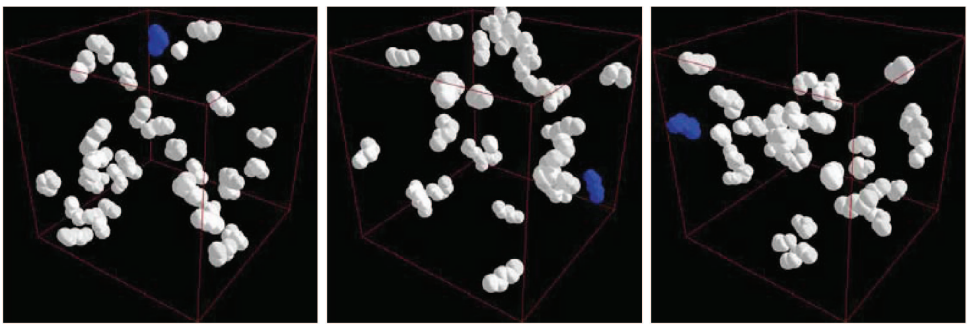

(a)At $t = 50t_{\sigma_{\mathrm{mol}}}$ (b)At $t = 75t_{\sigma_{\mathrm{mol}}}$ (c)At $t = 95t_{\sigma_{\mathrm{mol}}}$

FIG. 2. Time evolution for a system of $N = 32$ nC$_5$ molecules at $\rho = 0.2\rho_c$ with potential parameters from the AUA2 model over the course of the simulation in terms of the relaxation time of the molecular length scale $t_{\sigma_{\mathrm{mol}}}$.

length stretching or compressing (u_{bond}), bond-angle bending (u_{angle}), torsional-angle twisting owing to rotational energy barrier (u_{tors}), and non-bonded interactions that are described by the Lennard-Jones potential (u_{LJ}):[16,17]

$$u = u_{\text{bond}} + u_{\text{angle}} + u_{\text{tors}} + u_{\text{LJ}}, \tag{3}$$

where

$$u_{\text{bond}} = \sum_{N_{\text{bond}}} k_l (l - l_0)^2, \tag{4}$$

where N_{bond} is the number of bonds in the molecule, k_l is a proportionality constant, and l and l_0 are the actual and equilibrium bond lengths between two successive atoms, respectively;

$$u_{\text{angle}} = \frac{1}{2} \sum_{N_{\text{angle}}} k_\theta (\cos\theta - \cos\theta_0)^2, \tag{5}$$

where N_{angle} is the number of bond angles in the molecule, k_θ is a proportionality constant, and θ and θ_0 are the actual and equilibrium bond angles, respectively;

$$u_{\text{tors}}(\phi) = \sum_k a_k \cos^k(\phi), \tag{6}$$

where a_k are empirically determined coefficients; and

$$u_{\text{LJ}}(r_{ij}) = \begin{cases} 4\epsilon_{ij}\left[\left(\frac{\sigma_{ij}}{r_{ij}}\right)^{12} - \left(\frac{\sigma_{ij}}{r_{ij}}\right)^{6}\right] \\ -4\epsilon_{ij}\left[\left(\frac{\sigma_{ij}}{r_{\text{coff}}}\right)^{12} - \left(\frac{\sigma_{ij}}{r_{\text{coff}}}\right)^{6}\right], & \text{if } r_{ij} \le r_{\text{coff}} \\ 0, & \text{if } r_{ij} > r_{\text{coff}}, \end{cases} \tag{7}$$

where r_{ij} is the distance between interaction sites, r_{coff} is the cut-off distance for which the Lennard-Jones potential is truncated and shifted, and the energy ϵ_{ij} and length σ_{ij} potential parameters are determined from Lorentz-Berthelot mixing rules: $\epsilon_{ij} = (\epsilon_i \epsilon_j)^{1/2}$ and $\sigma_{ij} = (\sigma_i + \sigma_j)/2$. We use two sets of intermolecular potential parameters (Sec. II B) for Eq. (7) in our simulation. The Verlet neighbor list is also used.

We use the velocity Verlet algorithm[18–21] to update $\boldsymbol{r}_i$ and $\boldsymbol{v}_i = (dx_i/dt, dy_i/dt, dz_i/dt)$ at every time-step Δt. The velocities are scaled before measuring quantities to set the average energy $\langle E \rangle$ over starting times and over all molecules. Subsequently, we run the simulations at $E = \langle E \rangle$ and temperature fluctuates within a target mean $T_0 = T_c$.

We define three temperatures—atomic T_{atom}, molecular T_{mol}, and internal T_{int}—using the equipartition theorem, in terms of the atomic and molecular velocities:

$$T_{\text{atom}} = \frac{1}{3N_a - 3} \sum_{i=1}^{N_a} m_i (\vec{v}_i - \vec{V}_0)^2, \tag{8}$$

where the sum is over all atoms N_a and $\vec{V}_0$ is the velocity of the center of mass of all atoms in the system which is set to zero;

$$T_{\text{mol}} = \frac{1}{3N - 3} \sum_{j=1}^{N} M_j (\vec{V}_j - \vec{V}_0)^2, \tag{9}$$

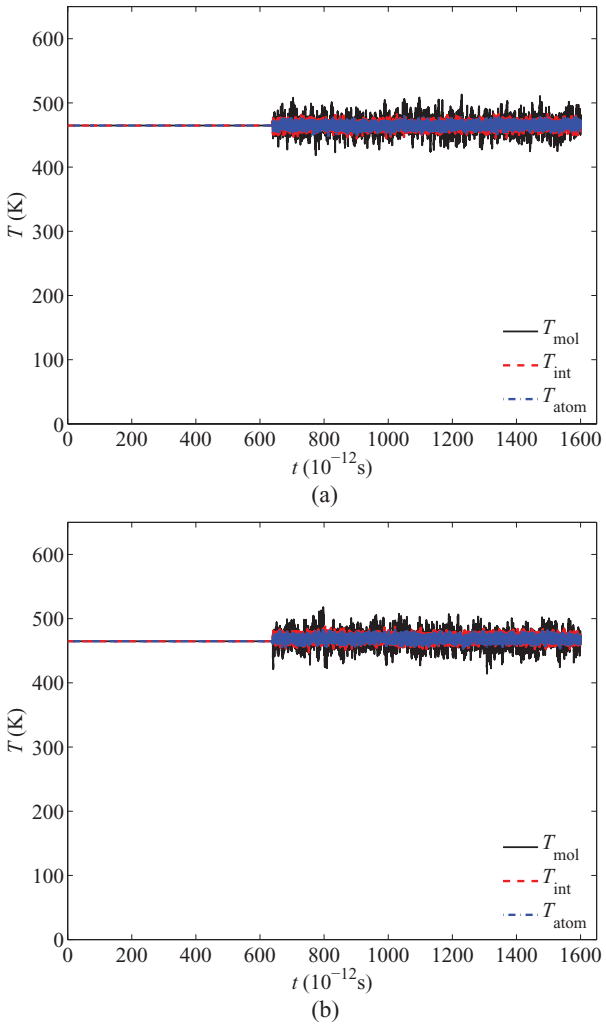

FIG. 3. Time histories of molecular, internal, and atomic temperatures for nC$_5$ at $\rho = \rho_c$ with potential parameters from (a) AUA1 and (b) AUA2 models, showing temperature equilibration at $T_0 = T_c$.

where the sum is over all molecules N; and M_j and $\vec{V}_j$ are the mass and velocity of the center of mass, respectively, of molecule j; and

$$T_{\text{int}} = \frac{1}{(3N_n - 3)N} \sum_{j=1}^{N} \sum_{i=1}^{N_n} m_i (\vec{v}_i - \vec{V}_j)^2, \tag{10}$$

where the sum is over all molecules N and over each atom N_n in the n-alkane molecule (i.e., 5 for nC$_5$).

During the initialization period, T_{atom} is scaled by $\sqrt{T_0/T_{\text{atom}}}$, where T_0 is the target temperature. As shown in the time histories in Figure 3, all three temperature measures equilibrate at the target temperature T_c.

The virial expression is used to calculate the pressure p:[20]

$$p = \frac{1}{V} \sum_{i=1}^{N} \left(T_{\text{mol}} + \frac{1}{3} \boldsymbol{R}_{\text{cm}_i} \cdot \boldsymbol{f}_i \right), \tag{11}$$

where $\boldsymbol{R}_{\text{cm}_i}$ is the location of the center of mass of molecule i.

The simulations in this work are performed with $\Delta t = 8.0 \times 10^{-16}$ s and $r_{\text{coff}} = 3.0\sigma_{ij}$. Sensitivity analysis with values

of $\Delta t < 8.0 \times 10^{-16}$ s and $r_{\text{coff}} > 3.0\sigma_{ij}$ was performed with no change in the results. The simulations were initialized with a face-centered cubic lattice with $N = 32$, 256, 500, and 1372 molecules, with the total simulation time varied depending on N. Most of the simulations were performed with $N = 256$ molecules, unless otherwise specified.

All the quantities are implemented in dimensionless form. The fundamental values are σ, ϵ, and m, from which all other units are derived, e.g., $t = \sigma\sqrt{(m/\epsilon)}\bar{t}$, $T = (\epsilon/k_B)\bar{T}$, etc. The resultant averaged quantities are converted to SI units.

B. Models

Two classes of collapsed atomic models—united atom (UA) and AUA—are often used for MD simulations of *n*-alkanes. Collapsed atomic models reduce the number of interaction sites and therefore the computation time without significant loss of accuracy. Lee *et al.*[22] showed that thermodynamic properties for liquid *n*-alkanes obtained from MD simulations with collapsed atomic models are comparable to those calculated from explicit atomic models.

In the UA model proposed by Ryckaert and Bellemans,[17,23] *n*-alkanes are modeled as chains of spheres whose interaction sites are on the carbon nuclei. The UA approach treats an *n*-alkane molecule as a group of monomers that are single-point-mass systems with no distinction between methyl ($-CH_3$) and methylene ($-CH_2-$) groups. Smit *et al.*[24] used a combination of Gibbs-ensemble and configuration-bias Monte Carlo (MC) methods to test the accuracy of various UA models—optimized potential for liquid systems model proposed by Jorgensen *et al.*,[25] de Pablo model,[26] and the Toxvaerd model[27,28]—in predicting vapor-liquid equilibria. In general, they found that these UA models predicted phase behavior of *n*-alkanes with reasonable accuracy over a wide temperature range.

The AUA model introduced by Toxvaerd[27] is an extension of the UA model which takes into account the anisotropy of the interactions between $-CH_2-$ and $-CH_3$ groups. In the AUA model, the force center is shifted by δ from the carbon nuclei and placed between the carbon and the hydrogen atoms of a related group. Thus, the form of the non-bonded potential changes from that given in Eq. (7) to

$$u_{\text{LJ}}(R_{ij}) = \begin{cases} 4\epsilon_{ij}\left[\left(\dfrac{\sigma_{ij}}{R_{ij}}\right)^{12} - \left(\dfrac{\sigma_{ij}}{R_{ij}}\right)^{6}\right] \\ -4\epsilon_{ij}\left[\left(\dfrac{\sigma_{ij}}{R_{\text{coff}}}\right)^{12} - \left(\dfrac{\sigma_{ij}}{R_{\text{coff}}}\right)^{6}\right], & \text{if } R_{ij} \le R_{\text{coff}} \\ 0, & \text{if } R_{ij} > R_{\text{coff}}, \end{cases} \tag{12}$$

where the interaction site $\boldsymbol{R}_i$ is with respect to the center of mass $\boldsymbol{r}_i$ of atom i:

$$\boldsymbol{R}_i = \boldsymbol{r}_i + \delta\left[\frac{\boldsymbol{r}_i - 0.5(\boldsymbol{r}_{i+1} + \boldsymbol{r}_i)}{|\boldsymbol{r}_i - 0.5(\boldsymbol{r}_{i+1} + \boldsymbol{r}_i)|}\right]. \tag{13}$$

The AUA model introduces a displacement between the centers of non-bonded interaction force and the centers of mass of the united atoms; thus, indirectly taking into account the effects of hydrogen atoms. Figure 4 shows a sketch of the key parameters that mark the differences between UA and AUA models as compared to the atomic structure for nC$_5$.

We consider two AUA models in this work: AUA1 which is based on the potential parameters by Toxvaerd[29] and AUA2 whose potential parameters are given by Ungerer *et al.*[13] The intramolecular parameters are the same for AUA1 and AUA2; whereas, the potential parameters for the non-bonded interactions are different.[13,29] Note that the Lennard-Jones length for AUA1 is the same for $-CH_2-$ and $-CH_3$ groups; whereas, AUA2 has different values. Using both sets of potential parameters ensures that the results obtained are consistent for two treatments of intermolecular interactions which are integral to molecular clustering.

Toxvaerd[27] showed that MD simulations using the UA model do not give the correct predictions for temperature, pressure, and density for propane, nC$_5$, and nC$_{10}$, including in the coexisting gas-liquid region, for a given potential parameter set. Therefore, the AUA model was introduced and shown to perform more accurately for these thermodynamic variables. In a subsequent publication, Padilla and Toxvaerd[28] tested the sensitivity of D_s to intra- and inter-molecular interactions for nC$_5$ and nC$_{10}$ using both UA and AUA models and different torsion potentials. They reported that the approach

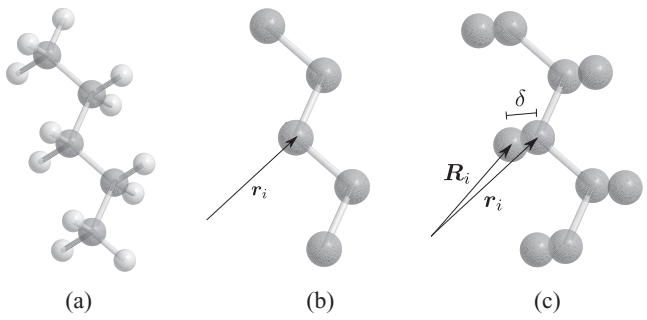

FIG. 4. A sketch (not to scale) of the (a) atomic structure, (b) united atom (UA) model, and (c) anisotropic united atom (AUA) model for nC$_5$. In the UA model (b), the non-bonded interaction site is centered on the carbon nuclei $\boldsymbol{r}_i$, while in the AUA model (c), the interaction site is shifted from $\boldsymbol{r}_i$ to $\boldsymbol{R}_i$ by a distance δ whose magnitude is different for the methyl and methylene groups.

that gave the best agreement of predicted D_s with experimental data for nC$_5$ and nC$_{10}$ was an AUA model (referred to as AUA$_{(2)}$ in their work), where the non-bonded interaction site was shifted by a different magnitude for the $-CH_2-$ and $-CH_3$ groups. We use the potential parameters for this model by Toxvaerd[29]—referred to as AUA1 in this work.

Ungerer *et al.*[13] optimized potential parameters for the Toxvaerd AUA model.[29] They tested the performance of their proposed model (referred to as AUA4 in their work) using Gibbs-ensemble MC, thermodynamic integration, and MD simulations. They reported that their optimized AUA model provides significant improvements for predictions of vapor pressures, vaporization enthalpies, liquid densities, and critical temperatures estimated from co-existence density curves. We test the performance of this optimized AUA model by Ungerer *et al.*[13]—referred to as AUA2 in this work.

C. Dynamics

In order to study the dynamics of n-alkanes in our simulations, we first characterized the system structure in both time and space by considering the space transform of the van Hove correlation—the intermediate scattering function $I(\boldsymbol{k}, t)$[30] whose self-part is given by

$$I(\boldsymbol{k}, t) = \langle e^{i\boldsymbol{k}\cdot(\boldsymbol{r}(t+\Delta t)-\boldsymbol{r}(t))}\rangle, \tag{14}$$

where $\langle\rangle$ represents the average over particles and time origins. The magnitudes of wave-vectors $\boldsymbol{k}$ are considered in terms of three length scales: Lennard-Jones length $2\pi/\sigma_i$, length of the n-alkane molecule $2\pi/\sigma_{\text{mol}}$, and length of the simulation box $n2\pi/L$.

Equation (14) gives information on the collective dynamics of the system, which establishes the appropriate simulation time for realistic dynamics to be obtained. Our simulation times are chosen to be about two orders of magnitude longer than the relaxation time of the molecular length scale obtained from Eq. (14). A typical plot of the correlation function $I(\boldsymbol{k}, t)$ over time is depicted in Figure 5 for nC$_5$ showing that the relaxation times of the three length scales are less than 2×10^{-11} s.

Having established the appropriate simulation time from the correlation function, we then consider the mean-squared displacement of the molecules $\langle r^2\rangle$:

$$\langle r^2(\Delta t)\rangle = \frac{1}{N}\left\langle \sum_i^N |\boldsymbol{r}_i(t+\Delta t) - \boldsymbol{r}_i(t)|^2 \right\rangle, \tag{15}$$

such that $\langle r^2\rangle$ was linear with time for all simulations as shown in Figure 6 for nC$_5$.

The translational self diffusion coefficient D_s in the long time regime—as depicted in Figure 7 for nC$_5$ at $\rho = \rho_c$—is extracted from $\langle r^2\rangle$ based on Einstein's relation:[31,32]

$$D_s(t) = \lim_{t\to\infty} \frac{1}{6t}\langle r^2(\Delta t)\rangle. \tag{16}$$

We use a modified *Amsterdam* method to quantify cluster formation: cluster size κ_{cl} in terms of the average number of molecules and the average number of clusters N_{cl} at a given cluster lifetime τ. The cluster lifetime τ tracks the minimum

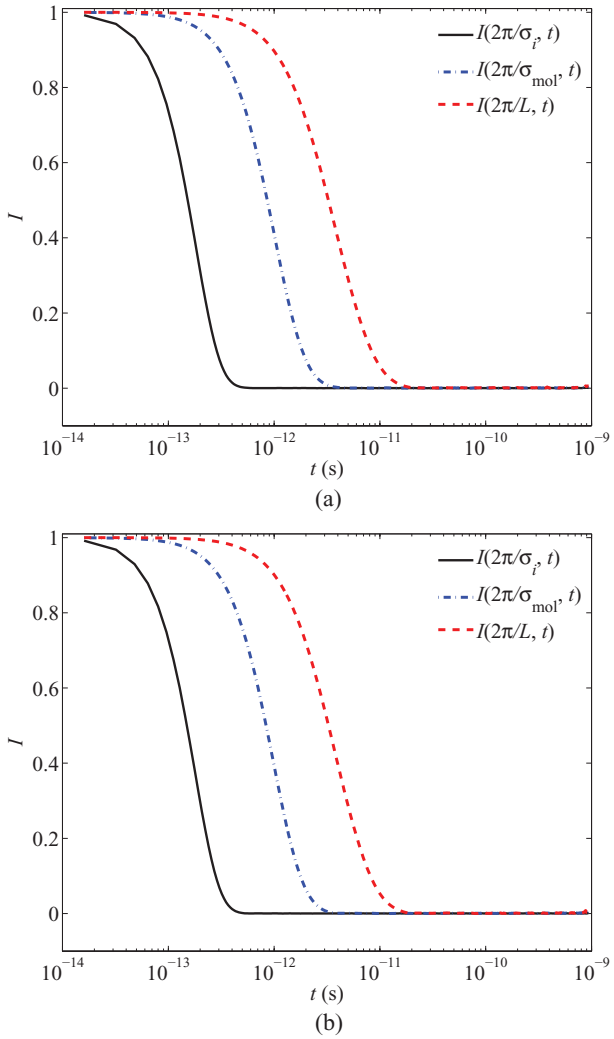

FIG. 5. Intermediate scattering function $I(\boldsymbol{k}, t)$ over time t for nC$_5$ at $\rho = \rho_c$ computed from (a) AUA1 and (b) AUA2 potentials. The relaxation times for nC$_5$ with respect to the three length scales is less than 2×10^{-11} s.

time that a cluster persists. The Amsterdam method is defined such that a molecule i is a nearest neighbor to a molecule j if $r_{ij} \le r_{\text{cl}}$ and molecule i belongs to a cluster if, and only if, it has at least four nearest neighbors and two neighboring molecules are in the same cluster.[33–35] Our modified algorithm considers two molecules to be neighbors if they have a monomer within a distance $r_{\text{cl}} = 1.5\sigma_{ij}$ of a monomer of the other molecule for a minimum time τ.

III. RESULTS AND DISCUSSION

A. Diffusion at experimental conditions

To the best of our knowledge, no D_s data are reported based on experimental measurements in the critical region of medium-chain n-alkanes considered in this work. However, we do test the predicted D_s from our MD simulations at some representative T and ρ conditions, outside of the critical regime, for which experimental data are available.

Table II summarizes the conditions for T and ρ at which experimental D_s data are available for nC$_5$, nC$_{10}$, and nC$_{12}$. The range of T and ρ indicate that the experimental data are

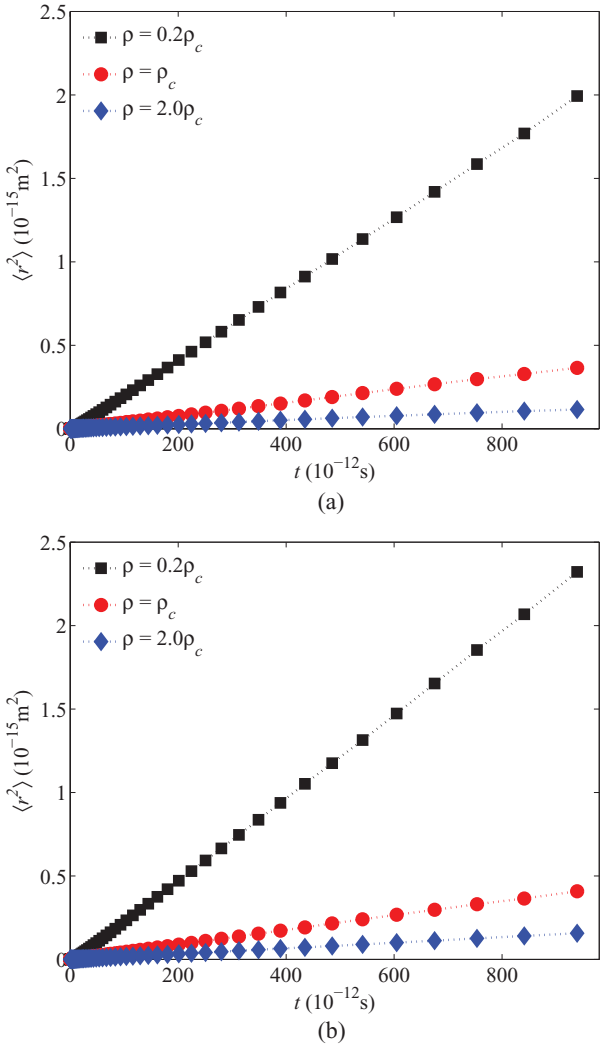

FIG. 6. Mean-squared displacement $\langle r^2 \rangle$ as a function of time t for nC$_5$ at three values of ρ computed from (a) AUA1 and (b) AUA2 potentials. Over the simulation time $t = 9.6 \times 10^{-9}$s, $\langle r^2 \rangle$ is linear with time.

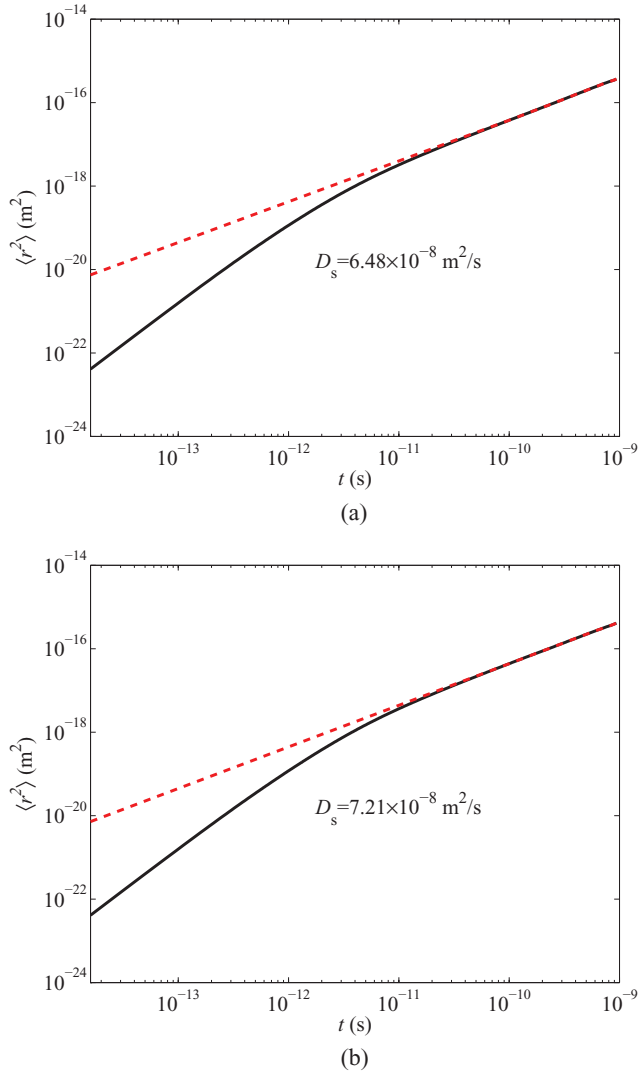

FIG. 7. Mean-squared displacement $\langle r^2 \rangle$ as a function of time t for nC$_5$ at $\rho = \rho_c$ from which D_s is determined for (a) AUA1 and (b) AUA2 potentials.

for systems in liquid phase state away from the critical conditions specified in Table I.

The performance of our MD simulations against some of these experimental data is shown in Table III. Note that where two or more data points are reported at the same conditions of T and ρ, an average is taken for comparison purposes. The D_s predictions with both AUA potential parameters are reasonably accurate. Overall, AUA1 predictions have an average dev = 7.5%, while AUA2 predictions have an average dev = 7.7%.

TABLE II. Summary of temperature T and density ρ conditions for which experimental self diffusion coefficients data of nC$_5$, nC$_{10}$, and nC$_{12}$ are available.[36–40]

n-alkane	T (K)	ρ (kg/m^3)
nC$_5$	$194.65 \le T \le 308.65$	$610.28 \le \rho \le 716.01$
nC$_{10}$	$293.15 \le T \le 313.15$	$714.87 \le \rho \le 730.41$
nC$_{12}$	$278.15 \le T \le 328.15$	$723.56 \le \rho \le 760.60$

TABLE III. Computed D_s from AUA1 and AUA2 models, and experimental data for nC$_5$, nC$_{10}$, and nC$_{12}$ at the temperature T and density ρ conditions given.

		D_s (10^{-9} m^2/s)			%dev	
T (K)	ρ (kg/m^3)	Expt.	AUA1	AUA2	AUA1	AUA2
		nC$_5$				
250.25	666.17	2.97[37]	3.17	2.96	6.8	0.5
273.15	644.95	4.14[37]	4.74	3.74	14.5	9.6
298.15	620.83	5.54[36,37]	6.12	6.18	10.5	11.6
308.65	610.28	6.29[37]	6.60	6.64	4.9	5.6
		nC$_{10}$				
293.15	730.41	1.44[38]	1.33	1.65	7.4	14.4
298.15	726.53	1.31[36,38,39]	1.49	1.66	3.1	14.7
303.15	722.64	1.68[38]	1.57	1.75	6.4	4.4
313.15	714.87	1.86[38]	1.73	1.88	6.8	0.9
		nC$_{12}$				
298.15	745.73	0.87[39,40]	0.94	0.95	8.3	8.8
308.15	738.33	0.97[40]	1.11	0.92	14.4	4.9
318.15	730.95	1.15[40]	1.23	1.29	6.4	12.1
328.15	723.56	1.34[40]	1.34	1.28	0.3	4.6

B. Diffusion in the critical region

Results in the critical region were obtained along critical isotherms $T = T_c$ over the density range $0.2\rho_c \leq \rho \leq 2.0\rho_c$ for each medium-chain *n*-alkane. In order to account for the differences in the critical density of the three *n*-alkane systems, the results are presented as functions of the reduced density in the form of $(\rho - \rho_c)/\rho_c$, with $(\rho - \rho_c)/\rho_c = 0$ marking the critical density.

1. Self diffusion coefficients

Figure 8 shows the predicted self diffusion coefficients D_s as the critical density is approached isothermally—from above and below ρ_c—for nC$_5$, nC$_{10}$, and nC$_{12}$ with $N = 256$ molecules. As shown, D_s for all three systems decreases with increasing density; a trend that is consistent even for non-critical isotherms (Appendix). No anomalous behavior can be observed near the critical density $(\rho - \rho_c)/\rho_c = 0$ where D_s remains finite. Note that in the literature, when anomalies in D_s have been observed in the critical region they are within 0.1%−20% of either ρ_c or T_c; when they are not seen they are

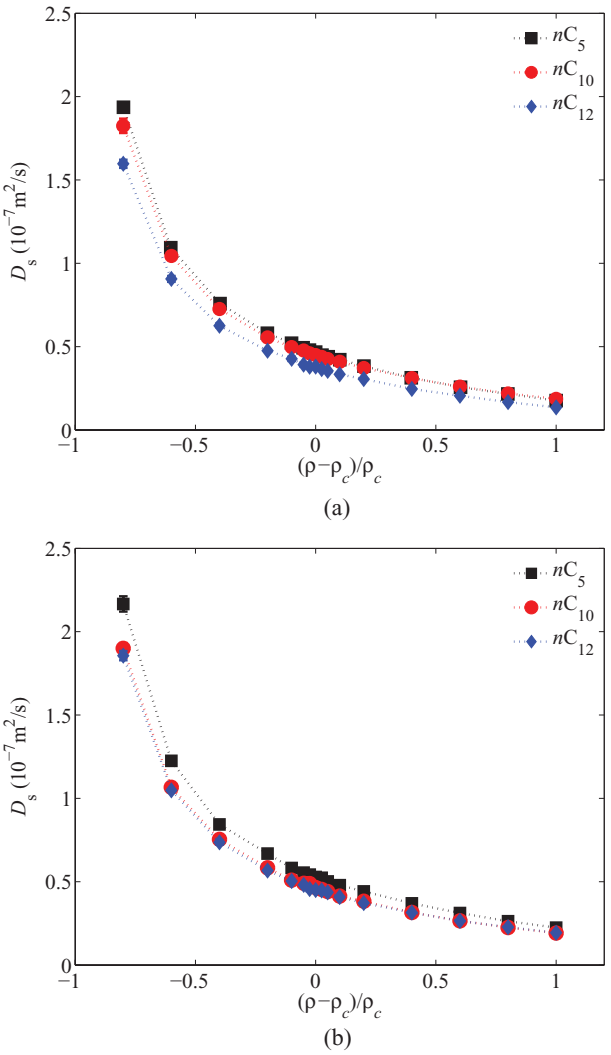

FIG. 8. Self diffusion coefficients D_s as functions of density $(\rho - \rho_c)/\rho_c$ for nC$_5$, nC$_{10}$, and nC$_{12}$ computed from (a) AUA1 and (b) AUA2 potentials.

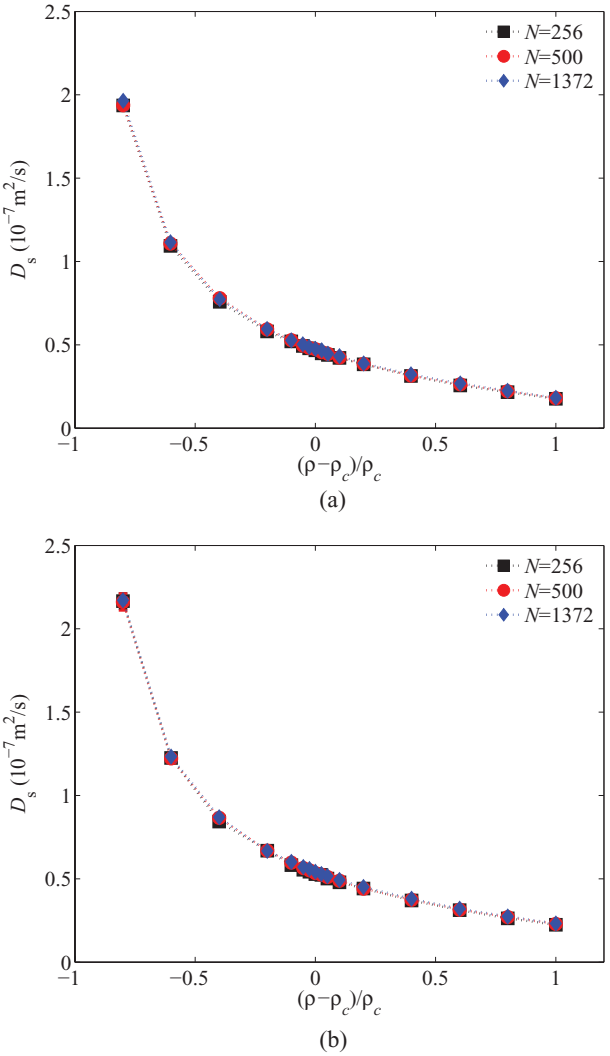

FIG. 9. Self diffusion coefficients D_s as functions of density $(\rho - \rho_c)/\rho_c$ for nC$_5$ at three system sizes $N = 256$, 500, and 1372 molecules computed from (a) AUA1 and (b) AUA2 potentials.

ruled out to within 1%−4% of either ρ_c or T_c. In this work, we rule out anomalies in D_s to within 2% of ρ_c.

In general, the AUA1 potentials give a lower magnitude of D_s than AUA2 potentials as shown in Figures 8(a) and 8(b), respectively. This may point to the importance of treating the interactions of $-CH_3$ and $-CH_2-$ groups differently through the Lennard-Jones length parameter. Furthermore, it is evident that D_s decreases with increasing length of the *n*-alkane from nC$_5$ to nC$_{12}$; a trend that is more pronounced at low densities $\rho < \rho_c$ (Figure 8). This is consistent with molecular mobility considerations where larger molecules are expected to diffuse slowly.

2. Investigation of finite size effects

Phase transitions occur in the thermodynamic limit where statistical degrees of freedom are unlimited. In finite systems, singularities of thermodynamic quantities at the critical point may be rounded to finite values necessitating finite-size scaling. Thus, in order to investigate finite size effects and ensure that the extracted D_s data are representative of infinite

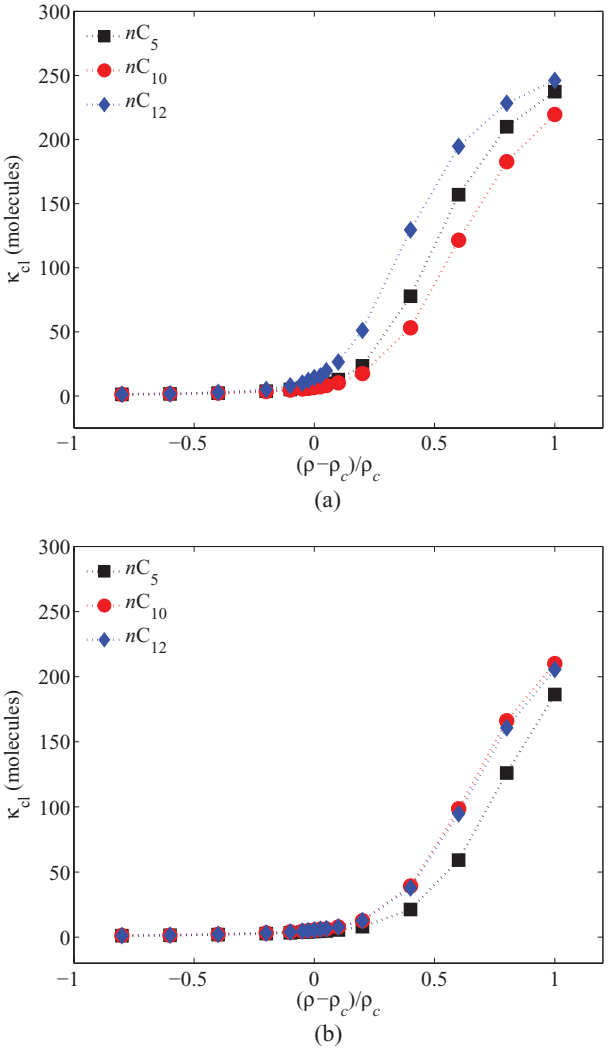

FIG. 10. Average cluster size κ_{cl} in terms of molecules over density $(\rho - \rho_c)/\rho_c$ for nC$_5$, nC$_{10}$, and nC$_{12}$ at a cluster lifetime of $\tau = 4.0 \times 10^{-13}$ s computed from (a) AUA1 and (b) AUA2 potentials.

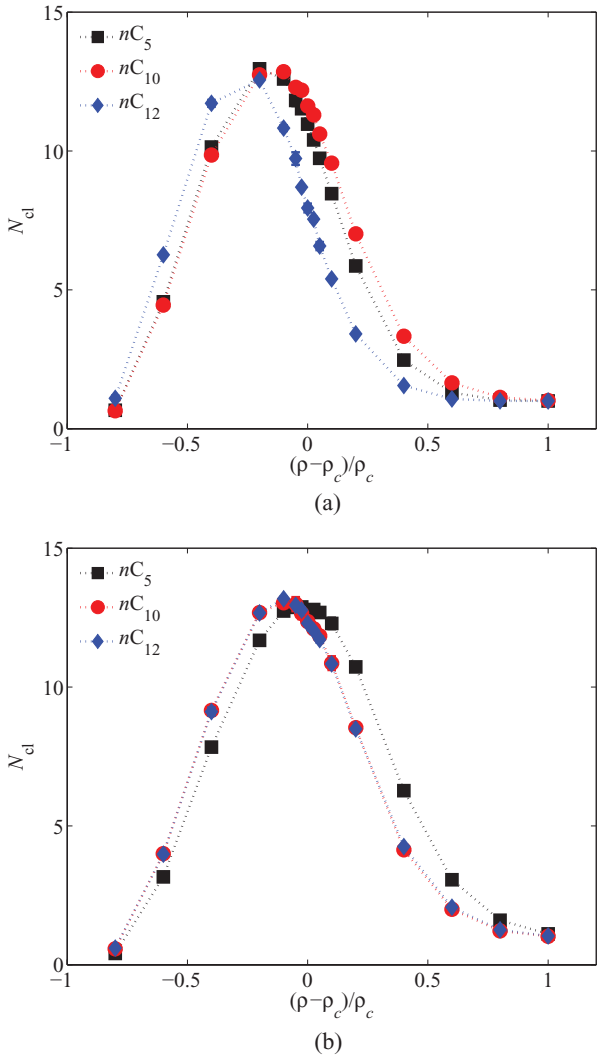

FIG. 11. Average number of clusters N_{cl} as functions of density $(\rho - \rho_c)/\rho_c$ for nC$_5$, nC$_{10}$, and nC$_{12}$ at a cluster lifetime of $\tau = 4.0 \times 10^{-13}$ s computed from (a) AUA1 and (b) AUA2 potentials.

systems, we performed simulations for nC$_5$ at increasing system sizes.

Figure 9 compares predictions of D_s for nC$_5$ at $N = 256$, 500, and 1372 molecules. No change in the magnitude of D_s can be observed over the entire range of density considered. The nearly identical values of D_s for nC$_5$ at increasing system sizes indicate that $N = 256$ molecules is sufficient for studying critical dynamics of medium-chain n-alkanes. Thus, we conclude that the finite nature observed in D_s at T_c and ρ_c is representative of single-component gas-liquid systems.

C. Cluster formation in the critical region

1. Cluster sizes and numbers

Figures 10 and 11 show the predicted average size of the clusters κ_{cl} in terms of the total average number of molecules and the average number of clusters N_{cl}, respectively, for nC$_5$, nC$_{10}$, and nC$_{12}$. The data are obtained at a cluster lifetime of $\tau = 4.0 \times 10^{-13}$ s.

As shown in Figures 10 and 11 for $\tau = 4.0 \times 10^{-13}$ s, κ_{cl} increases with increasing density which is consistent with decreasing D_s; whereas, N_{cl} reaches a maximum at a density $\sim 0.75\rho_c$. For all three n-alkanes, $\kappa_{cl} \geq 1$ molecule. Note that the trends in both κ_{cl} and N_{cl} change if a different cluster lifetime τ is used to track clustering behavior (Figures 12 and 13); at lower τ the curves shift to the left and at higher τ the curves shift to the right. Similar to D_s, no unusual behavior in either κ_{cl} or N_{cl} can be observed at the critical density. From molecular mobility considerations, the finite nature of κ_{cl} in the critical region supports a finite D_s.

Note that for a given n-alkane, the magnitude of κ_{cl} is larger with AUA1 (Figure 10(a)) potential parameters as compared to AUA2 (Figure 10(b)), which may explain the lower values of D_s predicted from AUA1 potentials (Figure 8). Further, the trend in both κ_{cl} and N_{cl} is non-monotonic with the length of the n-alkane with AUA1 potential parameters; whereas, with AUA2 potential parameters nC$_{10}$ and nC$_{12}$ have nearly identical molecular clustering behavior, but in comparison to nC$_5$ the expected monotonic trend is observed.

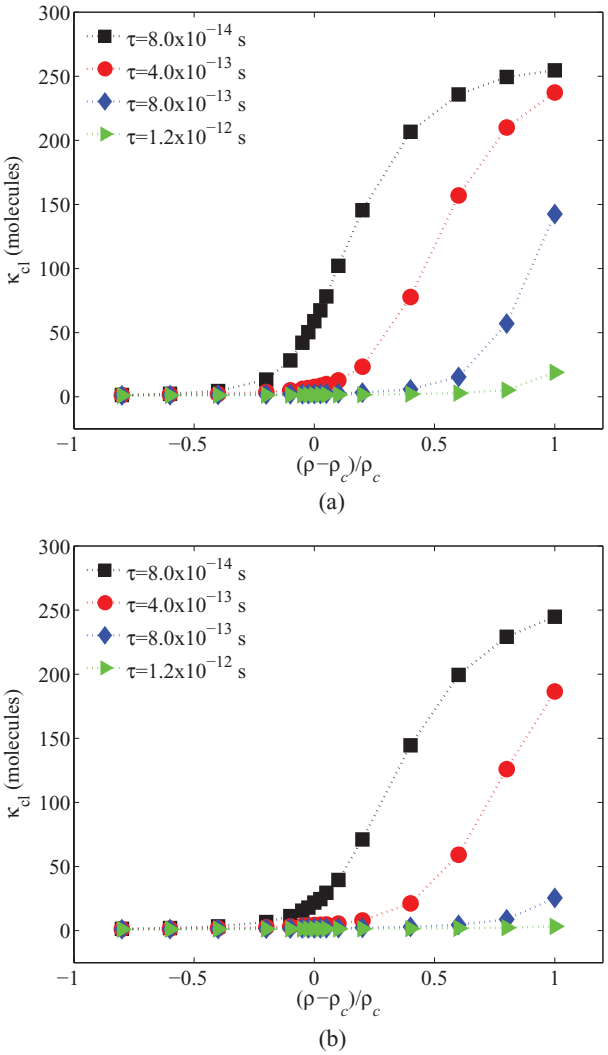

FIG. 12. Average cluster size κ_{cl} measured in terms of the number of molecules as functions of density $(\rho - \rho_c)/\rho_c$ for nC$_5$ at various cluster lifetimes τ in the range 8.0×10^{-14}s $\leq \tau \leq 1.2 \times 10^{-12}$ s computed from (a) AUA1 and (b) AUA2 potentials.

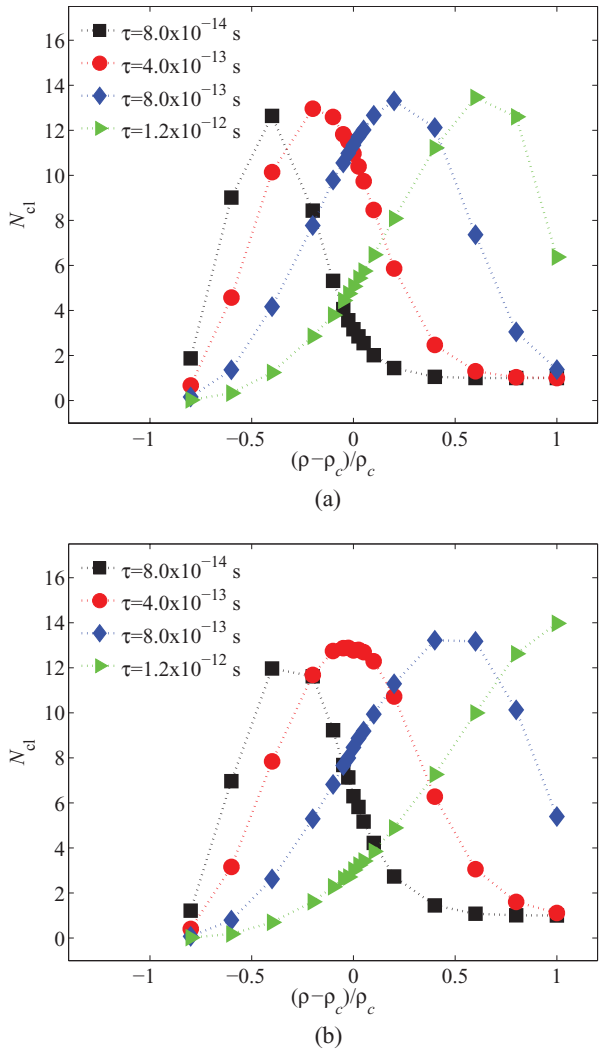

FIG. 13. Average number of clusters N_{cl} as functions of density $(\rho - \rho_c)/\rho_c$ for nC$_5$ at various cluster lifetimes τ in the range 8.0×10^{-14}s $\leq \tau \leq 1.2 \times 10^{-12}$ s computed from (a) AUA1 and (b) AUA2 potentials.

2. Cluster lifetimes

Figures 12 and 13 show the predicted average size κ_{cl} and number N_{cl} of the clusters for nC$_5$ at different cluster lifetimes in the range 8.0×10^{-14}s $\leq \tau \leq 1.2 \times 10^{-12}$ s. As shown, κ_{cl} decreases with a longer τ, but its trend—increasing κ_{cl} with increasing ρ—is consistent across all τ. Similarly, N_{cl} shifts its maximum towards higher density with increasing τ, indicating that clusters at higher density are more persistent. Persistence of molecular clusters at high density implies limited molecular motion; thus, lower D_s.

Cluster lifetime τ is a measure of duration for which molecular clustering persists. As evidenced by Figures 12 and 13, only a few clusters persist for $\tau > 8.0 \times 10^{-13}$ s at high density. Thus, for nC$_5$, we conclude that molecular clustering behavior is marked by formation of clusters of varying sizes and that are transient in nature. Similar trends were observed for nC$_{10}$ and nC$_{12}$. These observations are consistent with the strength of intermolecular forces at play in medium-chain n-alkanes, where molecular clustering is influenced by relatively weak London dispersion forces.

IV. CONCLUDING REMARKS

In this work, we perform extensive MD simulations to systematically investigate at the molecular-scale the behavior of self diffusion coefficients and molecular clustering along critical isotherms of medium-chain n-alkanes: n-pentane, n-decane, and n-dodecane. We quantify self diffusion coefficients using Einstein's relation and determine average molecular cluster sizes and numbers at various cluster lifetimes using the modified Amsterdam method.

We show that the self diffusion coefficient decreases as a function of density, remaining finite at the critical point. Consistently, the size of molecular clusters increases with increasing density and also remains finite at the critical point. Furthermore, the clusters formed are shown to be persistent for only short cluster lifetimes. Therefore, for medium-chain n-alkanes, the nature of molecular clustering is transient and is not limited to the critical region; instead, it is a function

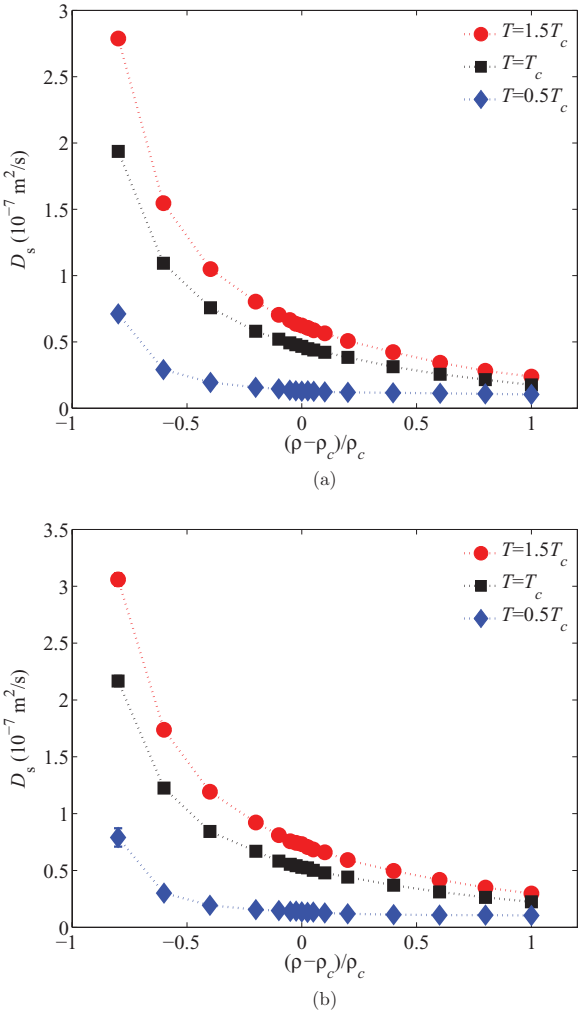

FIG. 14. Self diffusion coefficients D_s as functions of density $(\rho - \rho_c)/\rho_c$ for nC_5 at non-critical isotherms ($T > T_c$ and $T < T_c$) compared to the critical isotherm ($T = T_c$) computed from (a) AUA1 and (b) AUA2 potentials.

of density. Although slightly different D_s values are predicted with the two anisotropic united atom intermolecular potentials parameters considered, the trend is consistent across all three medium-chain *n*-alkanes. We conclude that there is no anomaly in the self diffusion coefficients, as confirmed by the transient nature of molecular clusters, in the critical region of single-component molecular fluids.

This work makes two fundamental contributions to critical phenomena studies: one, it confirms the continuity of self diffusion coefficients in the critical region of single-component molecular systems; and two, it provides a consistent molecular-scale basis for tracking the characteristics of transport coefficients in the critical region. A natural extension of this work is to binary systems where Fickian diffusion coefficients vanish in the critical region, but where molecular-scale understanding is still deficient.

ACKNOWLEDGMENTS

This work was supported in part by member companies of Reservoir Engineering and Research Institute (Palo Alto, California), and Yale University Faculty of Arts and Sciences High Performance Computing facility. C.S.O. acknowledges NSF-DMR-1006537 grant.

APPENDIX: DIFFUSION ALONG NON-CRITICAL ISOTHERMS

In the absence of persistent molecular clustering (as shown in Sec. III C) that could lower molecular velocities, the diffusion process is controlled by thermodynamic variables—temperature and density. At a constant density, we can show the temperature dependence of D_s by MD simulations at non-critical isotherms for the long time scales as indicated by Eq. (14).

Figure 14 depicts D_s along three isotherms: $0.5T_c$, T_c, and $1.5T_c$. As shown, D_s decreases with decreasing temperature, remaining finite at the reduced density $(\rho - \rho_c)/\rho_c = 0$. Furthermore, at low densities the differences in D_s for the three isotherms are more pronounced than at higher densities. These observations are consistent with kinetic theory considerations; at low temperature and high density, the kinetic energy of the molecules is lower, which limits the extent of molecular mobility.

[1]F. M. Orr, Jr. and J. J. Taber, Science **224**, 563 (1984).
[2]P. Oosting and N. Trappeniers, Physica **51**, 418 (1971).
[3]J. Noble and M. Bloom, Phys. Rev. Lett. **14**, 250 (1965).
[4]G. Cini Castagnoli, A. Longhetto, and D. Anfossi, Physica **49**, 153 (1970).
[5]J. S. Duffield and M. J. Harris, Ber. Bunsenges. Phys. Chem. **80**, 157 (1976).
[6]P. Etesse, A. M. Ward, W. V. House, and R. Kiboyashi, Physica B **183**, 45 (1993).
[7]A. N. Drozdov and S. C. Tucker, J. Chem. Phys. **114**, 4912 (2001).
[8]A. N. Drozdov and S. C. Tucker, J. Chem. Phys. **116**, 6381 (2002).
[9]K. R. Harris, J. Chem. Phys. **116**, 6379 (2002).
[10]S. K. Das, J. Horbach, K. Binder, M. E. Fisher, and J. V. Sengers, J. Chem. Phys. **125**, 024506 (2006).
[11]S. De, Y. Shapir, and E. H. Chimowitz, Chem. Eng. Sci. **56**, 5003 (2001).
[12]E. L. Cussler, AIChE J. **26**, 43 (1980).
[13]P. Ungerer, C. Beauvais, J. Delhommelle, A. Boutin, B. Rousseau, and A. H. Fuchs, J. Chem. Phys. **112**, 5499 (2000).
[14]*NIST Chemistry WebBook: NIST Standard Reference Database Number 69*, edited by P. J. Linstrom and W. G. Mallard (National Institute of Standards and Technology, Gaithersburg, MD, 2012), see http://webbook.nist.gov (retrieved March 13, 2012).
[15]R. L. Smith, Jr., A. S. Teja, and W. B. Kay, AIChE J. **33**, 232 (1987).
[16]P. C. Jurs, *Computer Software Applications in Chemistry*, 2nd ed. (Wiley, New York, 1996).
[17]J. P. Ryckaert and A. Bellemans, Faraday Discuss. Chem. Soc. **66**, 95 (1978).
[18]R. J. Sadus, *Molecular Simulation of Fluids: Theory, Algorithms and Object-Orientation* (Elsevier, Amsterdam, The Netherlands, 1999).
[19]D. C. Rapaport, *The Art of Molecular Dynamics Simulation*, 2nd ed. (Cambridge University Press, Cambridge, 2004).
[20]M. P. Allen and D. J. Tildesley, *Computer Simulation of Liquids* (Oxford University Press, New York, 2006).
[21]A. Satoh, *Introduction to Practice of Molecular Simulation: Molecular Dynamics, Monte Carlo, Brownian Dynamics, Lattice Boltzmann, Dissipative Particle Dynamics* (Elsevier, Burlington, 2011).
[22]S. L. Lee, H. Lee, H. Pak, and J. C. Rasaiah, Bull. Korean Chem. Soc. **17**, 735 (1996).
[23]J. P. Ryckaert and A. Bellemans, Chem. Phys. Lett. **30**, 123 (1975).
[24]B. Smit, S. Karaborni, and L. Siepmann, J. Chem. Phys. **102**, 2126 (1995).
[25]W. L. Jorgensen, J. D. Madura, and C. J. Swenson, J. Am. Chem. Soc. **106**, 6638 (1984).
[26]J. J. de Pablo, M. Laso, J. I. Siepmann, and U. W. Suter, Mol. Phys. **80**, 55 (1993).
[27]S. Toxvaerd, J. Chem. Phys. **93**, 4290 (1990).
[28]P. Padilla and S. Toxvaerd, J. Chem. Phys. **94**, 5650 (1991).

[29]S. Toxvaerd, J. Chem. Phys. **107**, 5197 (1997).
[30]J.-P. Hansen and I. R. McDonald, *Theory of Simple Liquids*, 3rd ed. (Academic, New York, 1986).
[31]D. A. McQuarrie, *Statistical Mechanics* (Harper & Row, New York, 1976).
[32]W. T. Coffey, Y. P. Kalmykov, and J. T. Waldron, *The Langevin Equation: With Applications to Stochastic Problems in Physics, Chemistry and Electrical Engineering*, 2nd ed., World Scientific Series in Contemporary Chemical Physics Vol. 14 (World Scientific, Singapore, 2004).
[33]P. R. ten Wolde and D. Frenkel, J. Chem. Phys. **109**, 9901 (1998).
[34]S. Sumardiono and J. Fischer, Int. J. Heat Mass Transfer **49**, 1148 (2006).
[35]B. A. Petrilla, M. F. Trujillo, and M. M. Micci, Atomization Sprays **20**, 581 (2010).
[36]D. C. Douglass and D. W. Mccall, J. Phys. Chem. **62**, 1102 (1958).
[37]E. Fishman, J. Phys. Chem. **59**, 469 (1955).
[38]J. W. Moore and R. W. Wellek, J. Chem. Eng. Data **19**, 136 (1974).
[39]B. A. Kowert, J. B. Jones, J. A. Zahm, and R. M. Turner II, Mol. Phys. **102**, 1489 (2004).
[40]M. Holz, S. R. Heil, and A. Sacco, Phys. Chem. Chem. Phys. **2**, 4740 (2000).